Received: 8 June 2020 | Revised: 10 April 2021 | Accepted: 13 April 2021

DOI: 10.1111/epi.16916

Epilepsia®

FULL-LENGTH ORIGINAL RESEARCH

Early onset epilepsy and sudden unexpected death in epilepsy with cardiac arrhythmia in mice carrying the early infantile epileptic encephalopathy 47 gain-of-function *FHF1(FGF12)* missense mutation

Jana Velíšková[1,2,3] | Christopher Marra[4,5] | Yue Liu[4,5] | Akshay Shekhar[6] | David S. Park[6] | Vasilisa Iatckova[4] | Ying Xie[4] | Glenn I. Fishman[6] | Libor Velíšek[1,3,7] | Mitchell Goldfarb[4,5]

[1]Department of Cell Biology & Anatomy and Department of Neurology, New York Medical College, Valhalla, New York, USA

[2]Department of Obstetrics and Gynecology, New York Medical College, Valhalla, New York, USA

[3]Department of Neurology, New York Medical College, Valhalla, New York, USA

[4]Department of Biological Sciences, Hunter College of City University of New York, New York, USA

[5]Program in Biology, Graduate Center of City University of New York, New York, USA

[6]Leon H. Charney Division of Cardiology, New York University School of Medicine, New York, USA

[7]Department of Pediatrics, New York Medical College, Valhalla, New York, USA

Correspondence
Jana Velíšková, Department of Cell Biology & Anatomy and Department of Neurology, New York Medical College, Valhalla, NY 10595, USA.
Email: jana_veliskova@nymc.edu

Mitchell Goldfarb, Department of Biological Sciences, Hunter College of City University, New York, NY 10065, USA.
Email: goldfarb@genectr.hunter.cuny.edu

Funding information
National Heart Lung and Blood Institute, Grant/Award Number: F31HL132438, R01HL105983 and R01HL142498; National Institute of Neurological Disorders and Stroke, Grant/Award Number: R01NS092786; Graduate Center, Grant/Award Number: 608100048, 802330016 and 945850101

Summary

Objective: Fibroblast growth factor homologous factors (FHFs) are brain and cardiac sodium channel-binding proteins that modulate channel density and inactivation gating. A recurrent de novo gain-of-function missense mutation in the *FHF1(FGF12)* gene (p.Arg52His) is associated with early infantile epileptic encephalopathy 47 (EIEE47; Online Mendelian Inheritance in Man database 617166). To determine whether the *FHF1* missense mutation is sufficient to cause EIEE and to establish an animal model for EIEE47, we sought to engineer this mutation into mice.

Methods: The Arg52His mutation was introduced into fertilized eggs by CRISPR (clustered regularly interspaced short palindromic repeats) editing to generate $Fhf1^{R52H/F+}$ mice. Spontaneous epileptiform events in $Fhf1^{R52H/+}$ mice were assessed by cortical electroencephalography (EEG) and video monitoring. Basal heart rhythm and seizure-induced arrhythmia were recorded by electrocardiography. Modulation of cardiac sodium channel inactivation by $FHF1B_{R52H}$ protein was assayed by voltage-clamp recordings of FHF-deficient mouse cardiomyocytes infected with adenoviruses expressing wild-type FHF1B or $FHF1B_{R52H}$ protein.

Results: All $Fhf1^{R52H/+}$ mice experienced seizure or seizurelike episodes with lethal ending between 12 and 26 days of age. EEG recordings in 19–20-day-old mice confirmed sudden unexpected death in epilepsy (SUDEP) as severe tonic seizures

immediately preceding loss of brain activity and death. Within 2–53 s after lethal seizure onset, heart rate abruptly declined from 572 ± 16 bpm to 108 ± 15 bpm, suggesting a parasympathetic surge accompanying seizures that may have contributed to SUDEP. Although ectopic overexpression of $FHF1B_{R52H}$ in cardiomyocytes induced a 15-mV depolarizing shift in voltage of steady-state sodium channel inactivation and slowed the rate of channel inactivation, heart rhythm was normal in *Fhf1*$^{R52H/+}$ mice prior to seizure.

Significance: The *Fhf1* missense mutation p.Arg52His induces epileptic encephalopathy with full penetrance in mice. Both *Fhf1* (p.Arg52His) and *Scn8a* (p.Asn1768Asp) missense mutations enhance sodium channel $Na_v1.6$ currents and induce SUDEP with bradycardia in mice, suggesting an FHF1/$Na_v1.6$ functional axis underlying altered brain sodium channel gating in epileptic encephalopathy.

KEYWORDS

bradycardia, CRISPR, EIEE47, FHF1(FGF12), SUDEP

1 | INTRODUCTION

Sudden unexpected death in epilepsy (SUDEP) accounts for up to 40% of all fatalities among individuals with therapeutically refractory epilepsy.[1,2] Risk for SUDEP is enhanced by early developmental onset of generalized seizures, in its severest form termed early infantile epileptic encephalopathy (EIEE). Causes underlying SUDEP are not easily revealed by postmortem examination, thereby restricting determination of mechanism to individuals undergoing polymodal physiological monitoring at time of death and to studies employing animal models. SUDEP may result from seizure-induced respiratory or cardiac arrest due to ictal or postictal firing anomalies in forebrain or brain stem regions controlling respiration and heart rhythm.[3–8] Alternatively, SUDEP may occur, in principle, independent of seizures due to genetic and developmental factors that may affect in parallel both seizure propensity and respiratory or cardiac dysfunction.

Causes of EIEE and SUDEP include mutations in genes encoding pore-forming subunits of voltage-gated sodium channels ($Na_v1.x$). Hemizygous loss-of-function mutations in *SCN1A* encoding $Na_v1.1$ (EIEE6) are the most common cause of human Dravet syndrome, a form of EIEE associated with myoclonic seizures occurring spontaneously or triggered by fever.[9,10] SUDEP in an *Scn1a*$^{+/-}$ mouse model of Dravet syndrome appears to be due to seizure-induced cardiac arrest triggered by parasympathetic cardiac suppression,[3,4,8] and breathing disorders in *Scn1a*-deficient mice have also been noted.[11] An *Scn1a* conditional loss-of-function mouse has been used to show that *Scn1a* deficiency in inhibitory neurons leads to epilepsy by increasing excitatory drive of neural networks.[12]

Key Points

- The heterozygous *FHF1* missense mutation Arg52His associated with EIEE47 causes seizures and SUDEP in juvenile mice
- Abrupt onset bradycardia in *Fhf1*$^{R52H/+}$ mice begins within seconds after the onset of terminal seizures
- SUDEP with bradycardia in *Fhf1*$^{R52H/+}$ mice bears similarity to lethality in *Scn8a*$^{N1768D/+}$ mice, paralleling similar effects of these mutations on inactivation gating of sodium channel $Na_v1.6$

In contrast, de novo heterozygous gain-of-function missense mutations of the *SCN8A* gene encoding $Na_v1.6$, (EIEE13) have been identified in more than 100 children with refractory infantile onset generalized seizures,[13–15] and some EIEE13 individuals succumb to SUDEP.[13] The mutant isoforms of $Na_v1.6$ protein have altered gating properties that are expected to increase sodium currents under physiological conditions and thereby enhance neuronal excitability.[16] Some of these mutations to $Na_v1.6$ channels, including $Na_v1.6$(N1768D), result in slower inactivation, a depolarizing shift in voltage dependence of steady-state inactivation, and elevated persistent sodium current,[13,17] whereas another EIEE13-associated mutation causes a hyperpolarizing shift in voltage-dependent activation.[18] In the EIEE13 mouse models *Scn8a*$^{N1768D/+}$ and *Scn8a*$^{N1768D/N1768D}$, animals undergo SUDEP brought on by tonic seizures[19] and have bradycardia due to enhanced tonic parasympathetic drive that worsens in the days preceding SUDEP.[20]

EIEE is also associated with mutations in genes encoding sodium channel-binding proteins. EIEE52, characterized by febrile and myoclonic seizures, is associated with homozygous deletion of the *SCN1B* gene encoding the beta-1 subunit of sodium channels.[21] EIEE47 involves mainly tonic and tonic–clonic seizures and is associated with a recurrent dominant missense mutation in the *FHF1(FGF12)* gene.[22–26] *FHF1* (fibroblast growth factor homologous factor 1) encodes cytosolic Na_v-binding proteins that are broadly expressed in neurons throughout the central nervous system, including the cerebral cortex, hippocampus, and brain stem.[27–33] FHF1A and FHF1B protein isoforms have different N-terminal moieties extending from a common β-trefoil core that includes the Na_v binding interface.[28,34–37] The EIEE47-associated arginine-to-histidine substitution within the FHF1 Na_v-binding domain ($FHF1A_{R114H}$, $FHF1B_{R52H}$) is gain-of-function with respect to $Na_v1.6$ modulation, such that the mutant isoforms induce greater depolarizing shifts in the voltage of steady-state inactivation than the wild-type protein counterparts.[22] Two children carrying the *FHF1* EIEE47 mutation experienced sudden death, whereas others have survived to date despite recurrent seizures. These findings show that epilepsy-inducing mutations in different genes, $SCN8A^{N1768D}$ and $FHF1^{R52H(R114H)}$, have similar effects on delaying $Na_v1.6$ inactivation.

Here, we report the generation and phenotypic characterization of mice heterozygous for the EIEE47 *Fhf1* missense mutation (abbreviated hereafter as $Fhf1^{R52H}$). All $Fhf1^{R52H/+}$ mice experience spontaneous seizures (epilepsy) and die of SUDEP at 12–26 days of age immediately following a terminal seizure episode. The terminal seizure onset is accompanied by sudden bradycardia, likely as the result of an autonomic surge. The comparison of our findings to prior studies on EIEE13 $Scn8a^{N1768D/+}$ mice[16,20] shows that dominant gain-of-function substitutions in $Na_v1.6$ or its binding partner FHF1 induce similar progression for epileptic encephalopathy, bradycardia, and SUDEP.

2 | MATERIALS AND METHODS

2.1 | DNA oligonucleotides

DNA oligonucleotides used were as follows:

F1-R52H-124b (for clustered regularly interspaced short palindromic repeats [CRISPR]-guided introduction of R52H and silent mutations): 5′-TTTTCTTTTCTTTTTTCCTTCTAGCCCTCTTCAATCTAATTCCTGTAGGACTGCACGTCGTCGCGATTCAGGGGGTTAAAGCCAGCCTTTATGTGGCCATGAATGGAGAAGGCTATCTCTACAG-3′;

F1-R52H-For (for polymerase chain reaction [PCR]): 5′-GTAGGACTGCACGTCGTCGCGATT-3′;

F1-IVS3-Rev (for PCR): 5′-GACTCACTCCATAGGGCATGA-3′;

F1-IVS2-For (for PCR): 5′-GCAGTGTGCCTCTCTTTGTGGTT-3′;

F1-Ex3-AS2 (for sequencing): 5′-CACACGACTGAACTTACTGAG-3′;

F1-R52H-S (mutagenesis): 5′-GAACCCCAGCTCAAAGGGTAATAGACAAGGTTATTCAGCCAGC-3′;

F1-R52H-AS (mutagenesis): 5′- GCTGGCTGAATAACCTTGTCTATTACCCTTTGAGCTGGGGTTC-3′;

F1-Delta-S (mutagenesis): 5′-CTAATTCCCGTGGGCCTGCATGTAGTGGCCATCCAAGG-3′; and

F1-Delta-AS (mutagenesis): 5′-CCTTGGATGGCCACTACATGCAGGCCCACGGGAATTAG-3′.

2.2 | CRISPR derivation of $Fhf1^{R52H/+}$ mice

All mice in these studies were generated, bred, and experimentally utilized under protocols approved by institutional animal care and use committees at Icahn School of Medicine at Mount Sinai, New York Medical College, New York

FIGURE 1 Generation and survival of $Fhf1^{R52H/+}$ mice. (A) Strategy for embryonic editing of the *Fhf1* gene. Reagents for gene editing were microinjected into pronuclei of fertilized eggs that were reimplanted into foster mothers to generate candidate founder mice. Two CRISPR (clustered regularly interspaced short palindromic repeats)-guided RNAs included sequences (shaded gray) near the Arg52 codon (shaded green) directing single-strand nicking by $Cas9_{D10A}$ at the adjacent protospacer adjacent motif (PAM) sites (shaded blue) on opposite DNA strands. Introduction of the R52H missense mutation (shaded pink) and six linked silent mutations (shaded yellow) were directed by mutagenic DNA oligonucleotide F1-R52H-124b. The sites corresponding to polymerase chain reaction (PCR) and sequencing oligonucleotides are indicated with arrows above the gene schematic. (B) PCR screening for pups bearing an $Fhf1^{R52H}$ allele. Genomic DNA was amplified with exon 3-flanking oligos F1-IVS2-For and F1-IVS3-Rev, and 500-base pair (bp) products were used as a template for PCR with F1-IVS3-Rev and F1-R52H-For, which only anneals without mismatch to the mutant allele sequence. Pups #5 and #86 yielded mutant diagnostic 270-bp products. (C) DNA sequencing of *Fhf1* alleles in first- and second-generation mice. The 500-bp amplicons spanning exon 3 from potential founder mice and progeny of mosaic Founder #5 were sequenced with primer F1-ex3-AS. $Fhf1^{R52H/+}$ Templates #86 and #5-22 showed heterozygosity at the seven edited residue sites, whereas Founder #5 is mosaic $Fhf1^{R52H/+}$: $Fhf1^{+/+}$, showing very weak representation of the mutant residues in chromatograms. The complementary sequences to the R52 and H52 codons are shaded green. $Fhf1^{R52H/+}$ heterozygotes from #5 and #86 founder lineages died as juveniles. (D) Survival of $Fhf1^{R52H/+}$ versus wild-type mice. All 91 $Fhf1^{R52H/+}$ mice, including 44 males and 47 females, died between postnatal Days 12 and 26, whereas all $Fhf1^{+/+}$ mice ($n = 200$) were viable. (E) Phenytoin delays death of $Fhf1^{R52H/+}$ mice. Residual survival time plot of $Fhf1^{R52H/+}$ mice administered phenytoin daily commencing on postnatal Day 12 ($n = 23$) versus untreated $Fhf1^{R52H/+}$ mice ($n = 68$). Phenytoin marginally, but significantly, extended survival time (treated 18.7 ± .4 days vs. untreated 16.1 ± .3 days, $p < .00005$)

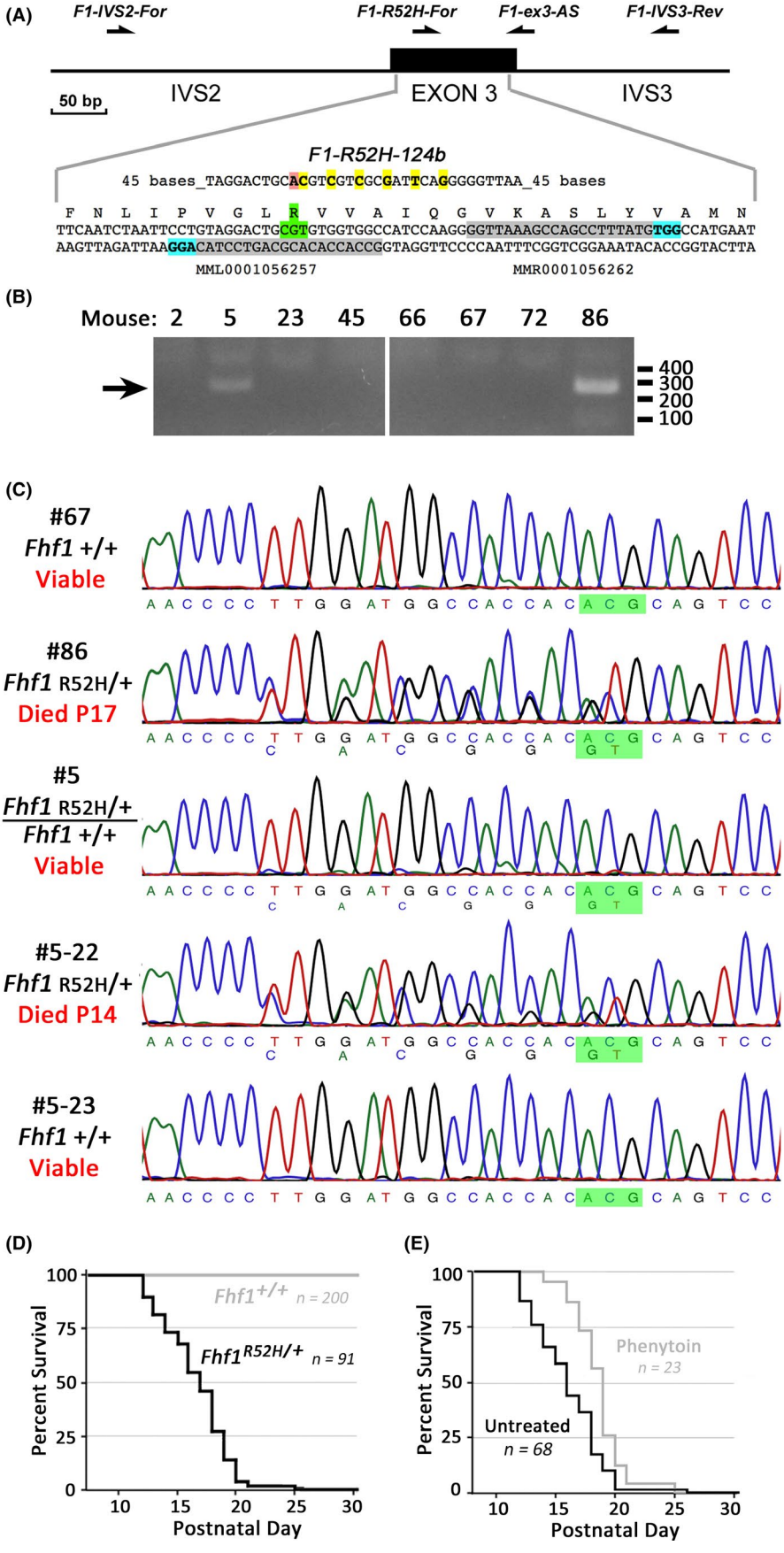
(A)
F1-IVS2-For
F1-R52H-For
F1-ex3-AS
F1-IVS3-Rev
50 bp
IVS2
EXON 3
IVS3
F1-R52H-124b
45 bases_TAGGACTGCACGTCGTCGCGATTCAGGGGGTTAA_45 bases
F N L I P V G L R V V A I Q G V K A S L Y V A M N
TTCAATCTAATTCCTGTAGGACTGCGTGTGGTGGCCATCCAAGGGGTTAAAGCCAGCCTTTATGTGGCCATGAAT
AAGTTAGATTAAGGACATCCTGACGCACACCACCGGTAGGTTCCCCAATTTCGGTCGGAAATACACCGGTACTTA
MML0001056257
MMR0001056262
(B)
Mouse: 2 5 23 45 66 67 72 86
400
300
200
100
(C)
#67
Fhf1 +/+
Viable
#86
Fhf1 R52H/+
Died P17
#5
Fhf1 R52H/+
Fhf1 +/+
Viable
#5-22
Fhf1 R52H/+
Died P14
#5-23
Fhf1 +/+
Viable
A A C C C C T T G G A T G G C C A C C A C A C G C A G T C C
(D)
Percent Survival
Postnatal Day
Fhf1+/+ n = 200
Fhf1R52H/+ n = 91
(E)
Percent Survival
Postnatal Day
Phenytoin
n = 23
Untreated
n = 68

University Langone Medical Center, and Hunter College of City University New York.

The *Fhf1*^{R52H} mutation was generated in mice by CRISPR editing via reagent pronuclear microinjection into F2 generation C57Bl/6 × DBA/2 fertilized eggs. Two guide RNAs (MML001056257 and MMR0001056262) and Cas9D10A nickase messenger RNA (Sigma-Aldrich) directed single-strand nicks at protospacer adjacent motif sites on opposite strands within *Fhf1* exon 3 flanking the Arg52 codon (Figure 1A), and the mutagenic DNA oligonucleotide F1-R52H-124b mediated the introduction of the R52H missense mutation together with six silent mutations into the *Fhf1* gene by homologous DNA strand invasion and repair (Figure 1A), as originally described.[38,39] Reimplantation of injected eggs into foster females yielded 98 progeny that were screened by PCR and DNA sequencing for successful mutagenesis.

2.3 | Genotyping and estimation of *Fhf1*$^{R52H/+}$: *Fhf1*$^{+/+}$ mosaicism in Founder Mouse #5

All thermal cycling employed Phire Hot Start DNA Polymerase and buffers (Thermo Fisher Scientific). Tail DNAs served as templates for unbiased amplification of a 500-base pair (bp) fragment spanning *Fhf1* exon 3 using PCR primers F1-IVS2-For and F1-IVS3-Rev (Figure 1A). Purified 500-bp amplicons were tested for the presence of the mutant allele by reamplification with nested mutant primer F1-R52H-For, which yielded a positive diagnostic 270-bp product for two of the 98 progeny (Figure 1A,B). The presence of the mutant allele in these pups and in the progeny of mosaic Founder #5 was confirmed by sequencing of the 500-bp amplicon with primer F1-Ex3-AS2 (Figure 1A). Male Founder #5 was mated with 129/SvPas females to derive *Fhf1*$^{R52H/+}$ and wild-type experimental animals. At age 16 months, mosaic Founder #5 was sacrificed, and sperm was cryopreserved for further propagation of the mutant allele by in vitro fertilization and reimplantation into foster mothers. The percentage of *Fhf1*$^{R52H/+}$ germ cell precursors in Mouse #5 was calculated as twice the percentage of *Fhf1*$^{R52H/+}$ offspring. Mosaicism in somatic tissues was approximated by comparing sequence chromatograms of 500-bp amplicons derived from these tissues to those of *Fhf1*$^{R52H/+}$ and wild-type offspring. The ratio of peak amplitudes for adjacent identical residues in wild-type DNA versus that for these residues in *Fhf1*$^{R52H/+}$ DNA, where one of these peaks was reduced by an introduced silent mutation, provided a consistent metric against which the ratio of these peak amplitudes in a #5 mosaic tissue could be compared to assess level of mosaicism. The percentage of mosaicism was taken from the analysis of three nucleotide doublets affected by silent mutations.

2.4 | Long-term video monitoring of nursing pups

Litters containing a mother with *Fhf1*$^{R52H/+}$ and wild-type pups were placed in the circular recording cage with regular nesting material, food ad libitum, and a tap water source. One or two infrared (IR) cameras were positioned above and/or on the side of the cage for continuous recordings under standard 12-h light/12-h dark cycling (lights on at 7:00 a.m.). Mice were recorded continuously until all mutants had died. Some pups were administered the antiseizure drug phenytoin (50 mg/kg intraperitoneal daily) between postnatal Days 11 and 18 in an attempt to delay lethality.

2.5 | Surgeries for electroencephalogram and simultaneous electroencephalogram/electrocardiogram

All surgeries were performed at postnatal Day 19. Epidural silver ball electroencephalographic (EEG) electrodes attached to a cranial tower (Figure 2A) were implanted as previously described.[40] Briefly, each pup was subjected to deep isoflurane anesthesia continuously monitored as lack of response to tail and paw pinch (induction 5% in oxygen; maintenance 3% in oxygen), and placed in a stereotaxic apparatus (Heinrich Kopf) with anesthesia mask attached. After cleaning the skull, four small openings were made bilaterally over the frontal and occipital cortices using a 19-gauge needle, and silver ball electrodes were placed into these openings onto the cortex and attached to a six-pin dual-in-line connector with .125-mm silver wire. Jeweler screws with silver wire attached were secured in the nasal bone and above the cerebellum to provide reference (nasal) and ground (cerebellum) electrodes. These screws also served as anchors for the dental acrylic cap. After recovery, the mouse was placed in a recording chamber with food and water supply, attached to the video and EEG recording systems, and recorded continuously under IR illumination. The procedure for implantation of both EEG and electrocardiographic (ECG) electrodes was similar, only differing in the use of an eight-pin dual in-line connector allowing for two pins dedicated to ECG electrodes. These ECG electrodes (either insulated stranded stainless steel wire or Teflon-insulated silver wire) were inserted under the skin on the right pectoral muscle and on the left anterior chest surface at the fourth intercostal space, and secured with a single silk stitch as described elsewhere.[41] The ECG signal was recorded between the uninsulated tips of these leads.

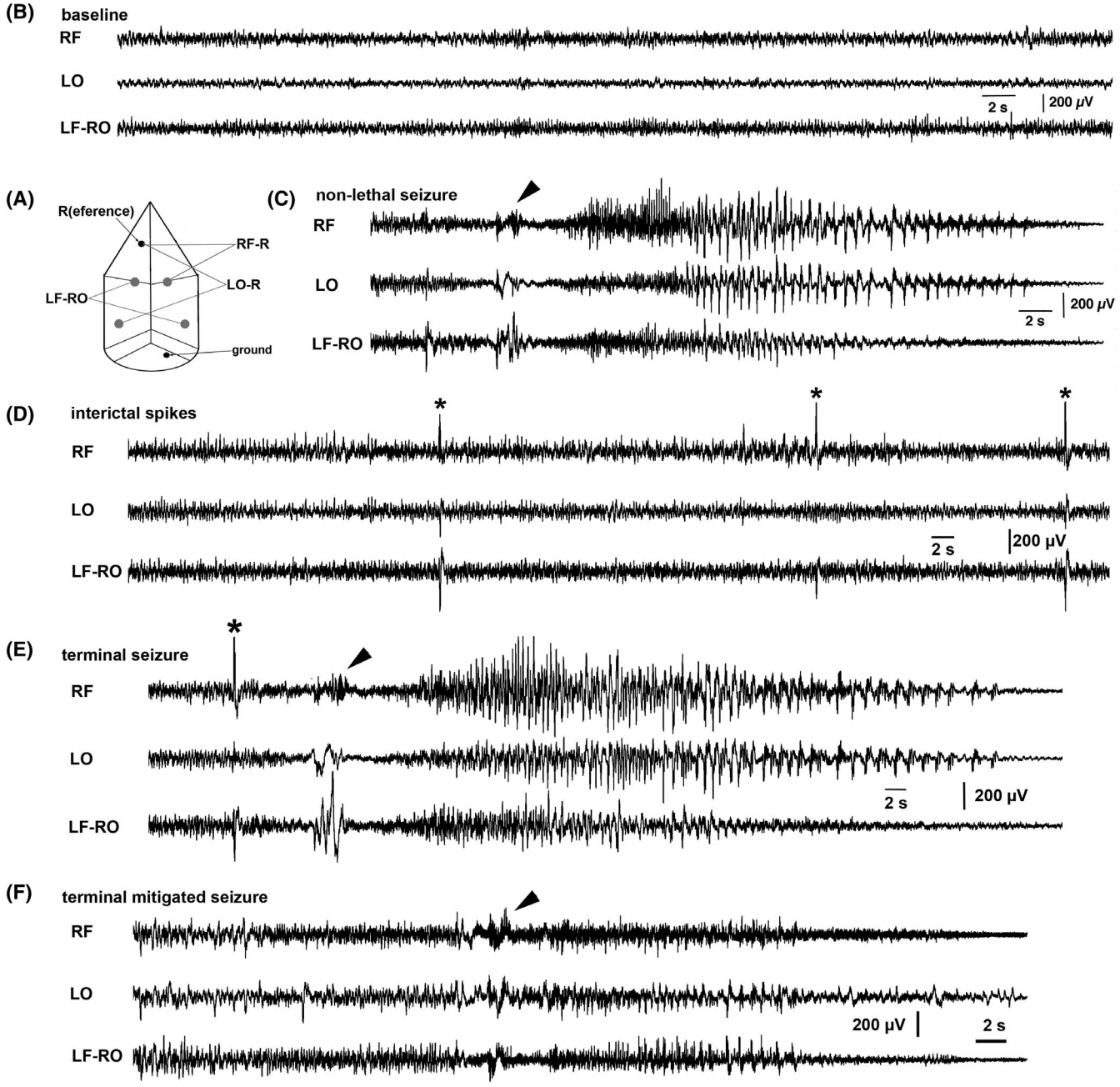

FIGURE 2 Electroencephalographic (EEG) recordings during nonlethal seizures, terminal seizures, and interictal periods in *Fhf1*$^{R52H/+}$ mice. (A) Scheme for all three-channel EEG recordings. RF (right frontal, sensorimotor) and LO (left occipital, visual) were unipolar mounts versus a reference electrode (R; an anchoring jeweler's screw) in the nasal bone. The third channel is LF-RO (left frontal vs. right occipital, a bipolar mount). Common ground was placed in the skull above the cerebellum (anchoring jeweler's screw). (B) Baseline recording during awake period. Low-amplitude fast activity beta waves were abundant in all channels. (C) A nonlethal seizure. This mutant mouse had four seizures between postnatal Day 19 (P19) and P21. One of the nonlethal seizures initiated coincident with a body twitch (arrowhead) followed by a tonic–clonic seizure with typical EEG signature consisting of fast spikes followed by spike-and-wave activity with slowing and decrease in amplitude and a period of postictal suppression (not shown). (D) Interictal spikes. The same animal as in C had frequent interictal spikes (asterisks) without behavioral correlates. (E) Terminal seizure. In the same animal as in C and D, a final interictal spike (asterisk) preceded a body twitch (arrowhead) and tonic–clonic seizure with fast spike and spike-and-wave phases indistinguishable from a preceding nonlethal seizure (C). (F) Terminal seizure with muted EEG signature. This mutant experienced near-identical behavioral signature preceding death as in E, commencing with body twitch (arrowhead) and a similar late spike-and-wave phase, but fast spikes were not readily detected

2.6 | Simultaneous EEG, ECG, and video recordings

We used a tethered Pinnacle Technology system with Sirenia 1.7.10-2.0.8 software. The EEG recording arrangement is shown in Figure 2A. Signals from the right frontal and left occipital electrodes were recorded against the reference electrode. Signal from left frontal electrode was recorded in bipolar arrangement against the signal from the right occipital electrode. For EEG-only recordings, signals were sampled at 800 Hz and subjected to 100-Hz low-pass and 1-Hz high-pass filtering. For simultaneous EEG/ECG recordings, signals were sampled at 5 kHz, with the same filtering as above for EEG traces and with 2-kHz low-pass and 1-Hz high-pass filtering for ECG traces. Mice were individually placed into circular recording cages with overhead cameras with IR illumination for continuous recordings.

2.7 | EEG and ECG evaluation

For off-line data evaluation, we first scanned video recordings to identify the terminal seizure event. Then, EEGs were visually inspected between the recording onset and the terminal point determined by the video recording. Clear EEG ictal activity was replayed with the video and correlated to behaviors. ECG data collected together with EEG data were evaluated off-line. Baseline heart rate in beats per minute (bpm) was sampled and averaged over a 6-h period subsequent to recovery from surgery anesthesia-induced bradycardia. PR interval was measured as the time between P and R peaks and averaged over 10 beats. Instantaneous heart rate in bpm at time $t_{(n)}$ seconds for beat n is calculated as $\text{bpm} = 60 \div \{t_{(n)} - t_{(n-1)}\}$. Surgical anesthesia suppressed heart rate in some mice for 1–3 h following awakening and initiation of recording. Therefore, EEG and ECG data were not analyzed until heart rhythm had stabilized.

2.8 | $FHF1B_{R52H}$ modulation of Na_v gating in cardiomyocytes

The human FHF1B coding sequence was cloned into the bicistronic adenovirus shuttle vector pAdTrack-CMV[42] to create pAdTrack-FHF1B/green fluorescent protein (GFP). QuikChange mutagenesis was used with mutagenic primers F1-R52H-S and F1-R52H-AS to generate pAdTrack-$FHF1B_{R52H}$/GFP or with primers F1-Delta-S and F1-Delta-AS to generate pAdTrack-$FHF1B_{DELTA}$/GFP, the latter of which has nonsense stop codons Ile11stop/Val12stop, thereby serving as negative control. In vivo recombination of shuttle vectors with pAdEasy-1 was performed in *Escherichia coli*, and resultant full-length adenoviral plasmids were linearized with PacI by standard procedure[42] and transfected via Lipofectamine 2000 (Life Sciences) into HEK293 cells to produce virus particles, which were purified and concentrated using Adeno-X Maxi kits (Takara Bio USA). FHF-negative dissociated ventricular cardiomyocytes from $Fhf2^{-/Y}$ mice were prepared as described previously,[43] plated onto poly-L-lysine/laminin-coated coverslips as described elsewhere,[44] and infected with the adenoviruses dually expressing FHF1B and GFP. Recordings were conducted 2–3 days postinfection from a Nikon electrophysiology workstation using a MultiClamp 700 amplifier, a Digidata analog/digital converter, and pClamp10 command and data acquisition software (Molecular Devices). Patch pipettes with resistance of 1–2 MΩ were filled with 135 $\text{mmol}\cdot\text{L}^{-1}$ CsF, 5 $\text{mmol}\cdot\text{L}^{-1}$ NaCl, 10 $\text{mmol}\cdot\text{L}^{-1}$ EGTA, 5 $\text{mmol}\cdot\text{L}^{-1}$ Mg-ATP, 15 $\text{mmol}\cdot\text{L}^{-1}$ hydroxyethylpiperazine ethane sulfonic acid (HEPES), pH 7.2 and used to attain voltage-clamped whole-cell patch access into GFP-fluorescent cardiomyocytes bathed in carbogen-bubbled 24 $\text{mmol}\cdot\text{L}^{-1}$ NaCl, 26 $\text{mmol}\cdot\text{L}^{-1}$ $NaHCO_3$, 50 $\text{mmol}\cdot\text{L}^{-1}$ choline-Cl, 25 $\text{mmol}\cdot\text{L}^{-1}$ tetraethylamine-Cl, 3 $\text{mmol}\cdot\text{L}^{-1}$ KCl, 3 $\text{mmol}\cdot\text{L}^{-1}$ CsCl, 12.5 $\text{mmol}\cdot\text{L}^{-1}$ 4-aminopyridine, 2 $\text{mmol}\cdot\text{L}^{-1}$ $MgCl_2$, 1 $\text{mmol}\cdot\text{L}^{-1}$ $CaCl_2$, 1 $\text{mmol}\cdot\text{L}^{-1}$ $BaCl_2$, .2 $\text{mmol}\cdot\text{L}^{-1}$ $CdCl_2$, 10 $\text{mmol}\cdot\text{L}^{-1}$ HEPES, pH7.2–11 $\text{mmol}\cdot\text{L}^{-1}$ D-glucose, 2 $\text{mmol}\cdot\text{L}^{-1}$ Na-pyruvate, 3 $\text{mmol}\cdot\text{L}^{-1}$ myoinositol. Cell capacitive and leak currents were subtracted through amplifier compensation and further during data acquisition by the pClamp P/N method. Voltage-dependence of Na_v steady-state inactivation was assayed using 50% series resistance compensation through a series of $n = 21$ consecutive command sweeps, each consisting of 60 ms at −150 mV, steady-state conditioning for 100 ms at $-150 + 5 \times (n-1)$ mV, and reporting for 20 ms at −30 mV. Peak inward sodium current for each sweep was generated at the reporting voltage by channels not inactivated by the conditioning voltage step. The $V_{1/2}$ voltage at which 50% of sodium channels underwent steady-state inactivation was determined by fitting data to a peak current versus voltage Boltzmann distribution. Rate of Na_v open-state inactivation was assayed from sodium current decay during voltage command steps from −150 mV to test voltages ranging from −35 to −10 mV. Current decays at each test voltage were fitted to a single-term exponential decay to determine time constant τ.

Cells infected with each of the three adenoviruses were lysed 48 h postinfection, and denatured proteins were electrophoresed through 4%–20% polyacrylamide gels (NuSep), transferred to polyvinylidene difluoride membranes, probed with antibodies specific for GFP (Abcam) or to FHF1 (Proteintech) proteins, and visualized by enhanced chemiluminescence.

2.9 | Statistics

Statistical significance of differences for ECG parameters in wild-type versus $Fhf1^{R52H/+}$ mice was analyzed by two-tailed

Student *t*-test. Similarly, differences in cardiomyocyte Na_v $V_{1/2}$ steady-state inactivation and open-state inactivation rate in cardiomyocytes infected with FHF1B versus $FHF1B_{R52H}$ adenovirus were analyzed by the *t*-test.

To reject the hypothesis that an off-site CRISPR-induced mutation unlinked to the *Fhf1*^{R52H} mutation was responsible upon inheritance for juvenile lethality, we employed Poisson distribution to calculate the probability $p = e^{-.5n}$ that none of *n Fhf1*$^{R52H/+}$ mice are viable.

3 | RESULTS

3.1 | Generation of *Fhf1*$^{R52H/+}$ mice

To confirm that the de novo missense mutation of the *FHF1* gene detected in multiple cases of human EIEE47 is sufficient to cause early onset epilepsy, the *Fhf1* mutation was recapitulated in mice by CRISPR editing.[38,39] Fertilized eggs received a mixture of $Cas9_{D10A}$ nickase mRNA, two guide RNAs targeting complementary DNA strands within *Fhf1* exon 3, and a mutagenic single-strand DNA oligonucleotide specifying the desired arginine → histidine substitution ($FHF1A_{R114H}$, $FHF1B_{R52H}$) along with six wobble silent mutations in adjacent codons to facilitate PCR genotyping (Figure 1A). Reimplantation of injected eggs into pseudopregnant females led to the birth of 98 pups, and PCR screening with a primer specific for the mutant *Fhf1* allele generated a product of predicted size in DNA from two founder mice, #5 and #86 (Figure 1B). The presence of the mutant allele in the founders was confirmed by unbiased PCR amplification spanning the targeting site in exon 3 followed by DNA sequencing. *Fhf1* exon 3 amplified from Founder #86 had a sequence read consistent with heterozygosity of wild-type and R52H mutant alleles, with two overlapping peaks at the seven targeted residues (Figure 1C). In contrast, the sequence of *Fhf1* exon 3 amplified from Founder #5 suggested mosaicism of heterozygous and wild-type homozygous cells, with the seven targeted residues showing very weak representation of the mutant allele in tail DNA (Figure 1C). After later sacrifice of this animal, heart, brain, and skeletal muscle DNA also showed weak representation of the mutant allele. The sequence chromatograms allowed estimation of 12%–18% *Fhf1*$^{R52H/+}$ cells in somatic tissues in mosaic Founder #5 (see Materials and Methods for explanation).

The *Fhf1*$^{R52H/+}$ Founder #86 died suddenly and unexpectedly on postnatal Day 17 in an unrecorded event suggesting SUDEP, making propagation of the mutant allele dependent upon breeding from the putative mosaic male Founder #5. Breeding of Founder #5 gave rise to the heterozygous *Fhf1*$^{R52H/+}$ genotype in 91 of 398 offspring (22.8%), as confirmed by DNA sequencing of amplified *Fhf1* exon 3 (examples in Figure 1C). Hence, approximately 45% of germ cell precursors are *Fhf1*$^{R52H/+}$, constituting a much higher proportion of mutant cells compared with somatic tissues.

All 91 *Fhf1*$^{R52H/+}$ progeny died as juveniles at 12–26 days of age (average age of death = 16.7 ± .3 days; Figure 1D). The 100% lethality of mutant mice offers proof ($p < 10^{-10}$, see Materials and Methods) that lethality is not due to an off-site CRISPR-induced mutation in mosaic Founder #5. Except for seizure or seizurelike episodes (see below), mutant mice had normal body weight and showed no overt signs of morbidity. By contrast, no wild-type littermates died as juveniles (Figure 1D). Daily administration of the antiseizure drug phenytoin (daily 50 mg/kg) to *Fhf1*$^{R52H/+}$ mice minimally, but significantly, prolonged survival (treated 18.7 ± .4 days $n = 23$ vs. untreated 16.1 ± .3 days $n = 68$, $p < .00005$; Figure 1E).

3.2 | EIEE and SUDEP in *Fhf1*$^{R52H/+}$ mice

Litters containing 12–19-day-old *Fhf1*$^{R52H/+}$ pups were continuously monitored by IR video recording under standard 12-h light/12-h dark cycling. Twenty-five of 40 video-monitored *Fhf1*$^{R52H/+}$ pups that died prior to weaning underwent seizurelike episodes immediately preceding death. As shown in Video S1, mutant pups engaged in a brief running fit followed by a tonic phase from which they did not recover. The other mutant pups died while nesting under their mothers, obscuring their exact time and manner of death.

EEG recording in conjunction with video monitoring was performed in *Fhf1*$^{R52H/+}$ mice surviving through postnatal Day 19 ($n = 10$).[40] In some cases ($n = 6$), ECG was also recorded. EEG and video monitoring of *Fhf1*$^{R52H/+}$ mice all captured behavioral seizures associated with EEG ictal activity immediately preceding death (Figure 2). The EEG signatures were different among these animals. Eight *Fhf1*$^{R52H/+}$ mice exhibited a rapid succession of events: (1) sharp electrical spike; (2) a brief running fit coincident with a preictal waveform; (3) a tonic seizure with large spike and wave components; and (4) loss of brain activity within 60 s, signaling death (Figure 2E and Video S2). The other two *Fhf1*$^{R52H/+}$ mice exhibited similar time course of observable seizure, but with low-amplitude electrographic signatures (Figure 2F), suggesting that these seizures possibly emanated from deeper brain structures. These observations allow categorization of *Fhf1*$^{R52H/+}$ mortality as SUDEP coincident with seizure. Three of the mutant animals experienced additional recorded seizures and interictal spikes prior to terminal seizure (examples in Figure 2C,D).

3.3 | Sudden bradycardia during terminal seizure in *Fhf1*$^{R52H/+}$ mice

To distinguish among potential causes of seizure-induced death, the six *Fhf1*$^{R52H/+}$ mice implanted at 19 days of age

with EEG and ECG electrodes were monitored continually. All six mice suffered terminal seizure within 36 h of surgery and recording initiation. Eight wild-type mice with similar implants were viably maintained for at least 72 h before recording was terminated. *Fhf1*$^{R52H/+}$ instantaneous heart rates 5 s prior to seizure onset were 597 ± 14 bpm (Figure 3A). In all *Fhf1*$^{R52H/+}$ mice, instantaneous heart rate abruptly plunged to less than 160 bpm at times ranging from 3 to 53 s (median = 9 s) following EEG ictal activity onset (Figure 3A). Tonic extension commenced during all fatal seizures within 4 s before or after bradycardia onset (Figure 3B), suggesting that both events resulted from the arrival of depolarization to the brain stem.[8] Cessation of detectable cortical activity occurred between 30 and 100 s after onset of bradycardia and tonic extension, whereas slowed and irregular heart rhythm persisted for 3–9 min before cardiac arrest (data not shown).

Figure 3C shows the EEG and ECG data for one of these lethal seizures in greater detail. Seizure onset (arrow) marked by enhanced brain activity in all EEG channels was followed by abrupt decline in instantaneous heart rate to 73 bpm within 3 s. The slower heart rhythm over the first 20 s of seizure may represent ventricular beats, based upon absence of detectable P waves. These data show that seizures can induce sudden ictal bradycardia that may contribute to SUDEP in *Fhf1*$^{R52H/+}$ mice.

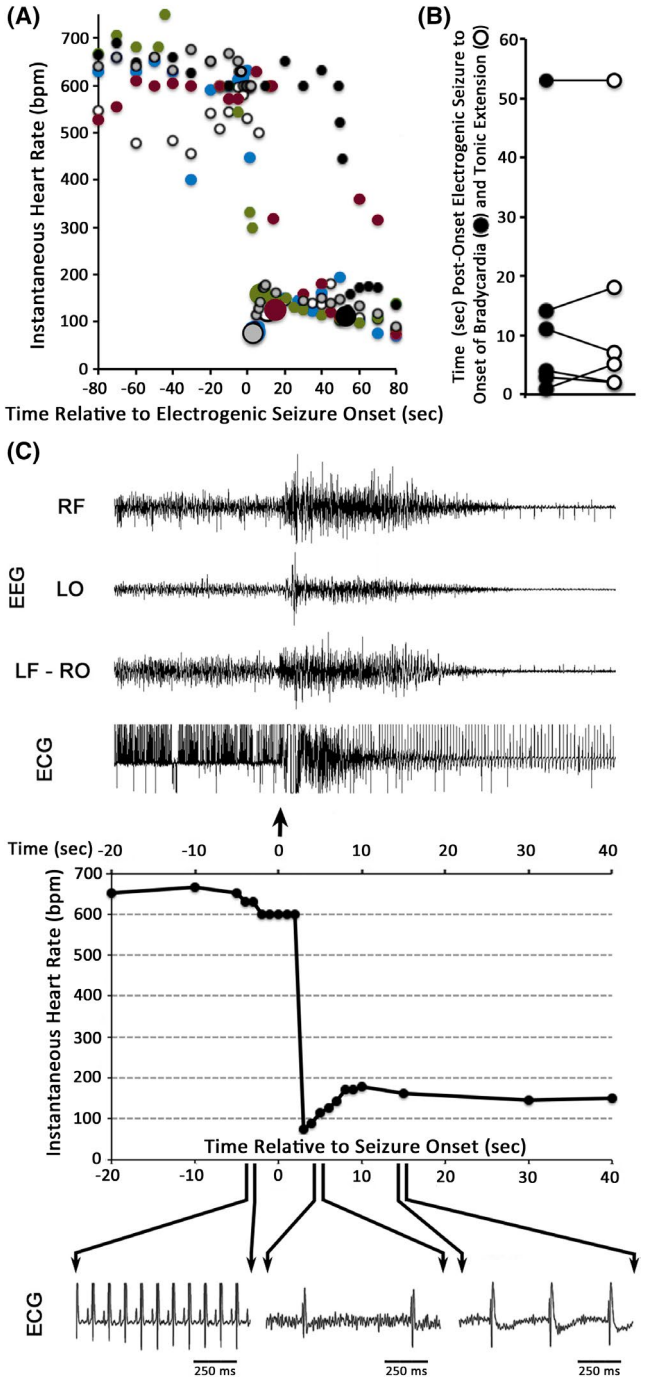

3.4 | Normal baseline cardiac rhythm in *Fhf1*$^{R52H/+}$ pups despite modulation of cardiac sodium currents by FHF1B$_{R52H}$

The FHF1B isoform encoded by the *Fhf1* gene is strongly expressed in mouse atrial cardiomyocytes as well as in brain[28,45] (and Shekhar and Fishman, unpublished data). Because FHF1B can bind to and modulate cardiac sodium channel $Na_v1.5$,[46] we investigated how R52H substitution in FHF1B alters Na_v gating in cardiomyocytes. Cultured FHF-deficient cardiomyocytes (see Materials and Methods) were infected with adenoviruses expressing GFP together with wild-type FHF1B, FHF1B$_{R52H}$, or no FHF, and sodium currents were assayed under voltage clamp protocols in fluorescent cells 2–3 days postinfection. FHF1B$_{R52H}$ induced a 15-mV right shift in Na_v steady-state inactivation (Figure 4A) and slowed

FIGURE 3 Sudden bradycardia at onset of terminal seizures in *Fhf1*$^{R52H/+}$ mice. (A) Instantaneous heart rates upon seizures. Heart rates for each of six *Fhf1*$^{R52H/+}$ mice are marked with different color circles before and after the onset of electrogenic seizure (time = 0). All lethal seizures were accompanied by abrupt decline in heart rate to ≤160 beats per minute (bpm), which is marked by a larger diameter circle, occurring in these mice at 3, 4, 7, 11, 15, or 53 s after onset of seizure. (B) Coincidence of tonic extension and bradycardia onset. For each of the six *Fhf1*$^{R52H/+}$ mice described in A, the time of bradycardia onset (closed circles) and tonic extension (open circles) are plotted and linked. Bradycardia and tonic extension always commenced within 4 s of one another, despite the wide temporal variability of these events relative to electrogenic seizure onset. (C) Abrupt suppression of cardiac rhythm by terminal seizure in an *Fhf1*$^{R52H/+}$ mouse. Top: Electroencephalographic (EEG) and electrocardiographic (ECG) traces from 20 s before to 40 s after seizure onset. The EEG channel designations are the same as described in Figure 2. The tonic seizure superimposes electromyographic noise on the ECG signal. Middle: Graph of instantaneous heart rate over the same time period as above shows abrupt drop in heart rate within 3 s of seizure onset. Bottom: One-second time scale enlargements of the ECG trace 4 s before and 4 or 14 s after seizure onset. The ECG waveform after bradycardia onset lacks detectable P waves, suggesting ventricular beats. LF-RO, left frontal versus right occipital; LO, left occipital; RF, right frontal

the rate of Na_v inactivation by more than twofold across a range of membrane potentials (Figures 4B and S1). In contrast, wild-type FHF1B expression at levels comparable to that of $FHF1B_{R52H}$ (Figure S1) did not significantly alter inactivation gating of cardiac sodium channels (Figures 4A,B and S1). Hence, $FHF1B_{R52H}$ is a gain-of-function modulator of both neuronal[22] and cardiac sodium channels.

The effect of $FHF1B_{R52H}$ substitution on gating of cardiac and neuronal sodium channels raised the possibility that heart rhythm in *Fhf1*$^{R52H/+}$ mice could be altered by cardiac-intrinsic or autonomic mechanisms. Basal heart rhythm was assessed in 19-day-old wild-type ($n = 8$) and *Fhf1*$^{R52H/+}$ ($n = 6$) mice implanted with an ECG electrode along with EEG electrodes. The ECG waveform in mutant mice prior to seizure was indistinguishable from that for wild-type (Figure 4C,D). Furthermore, average basal heart rates recorded over a 6-h period were not significantly different in mutant mice (Figure 4E), nor was the time delay between atrial and ventricular depolarization (PR interval, Figure 4F). The absence of a measurable intrinsic cardiac phenotype in *Fhf1*$^{R52H/+}$ mice likely reflects the restriction of endogenous FHF1 expression to atrial cardiomyocytes and the inability of single unipolar chest electrode recording to detect potentially subtle alterations in the P wave.

4 | DISCUSSION

All *Fhf1*$^{R52H/+}$ mice suffered seizures with a tonic component during the juvenile period, thereby providing the most compelling evidence to date that this recurrent missense mutation is sufficient to cause human EIEE disorder. Surprisingly, all *Fhf1*$^{R52H/+}$ mice suffered a terminal seizure at 2–4 weeks of age. This lethal phenotype was observed in *Fhf1*$^{R52H/+}$ Founder #86 and in all 91 *Fhf1*$^{R52H/+}$ progeny derived from mosaic Founder #5, thereby ensuring that early death was the

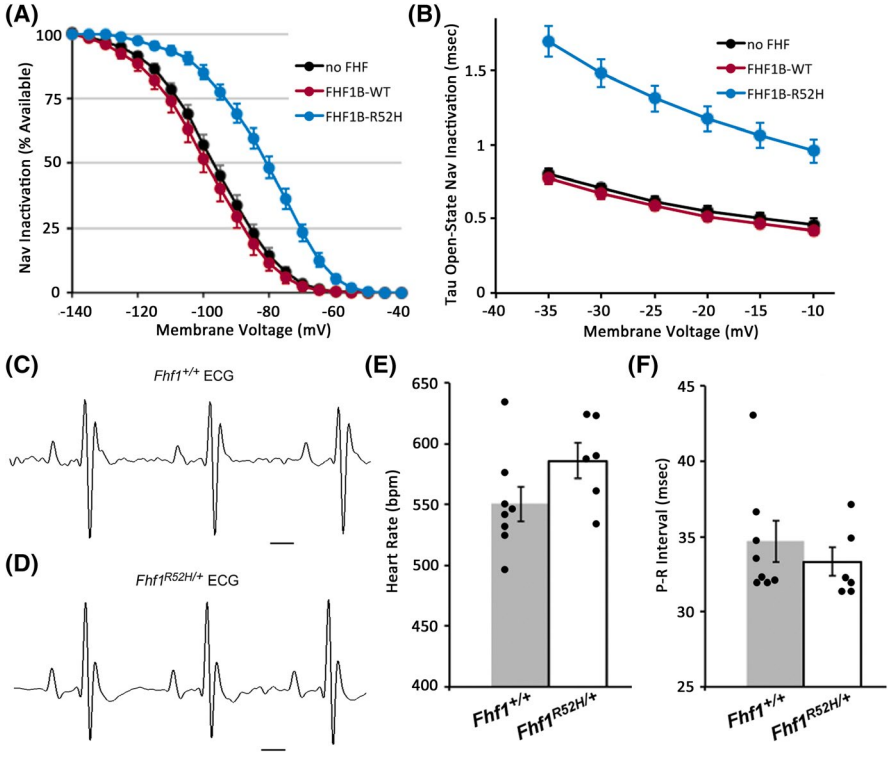

FIGURE 4 Effects of $FHF1_{R52H}$ on Na_v inactivation and basal heart function. (A) Ectopic $FHF1B_{R52H}$ in cardiomyocytes depolarizes the voltage dependence of Na_v inactivation. Dissociated adult ventricular cardiomyocytes from *Fhf2*$^{-/Y}$ mice were infected with adenoviruses expressing green fluorescent protein and either wild-type FHF1B, $FHF1B_{R52H}$, or no FHF. Sodium currents measured in fluorescent infected cells following equilibration at test membrane voltages were used to assess voltage dependence of steady-state Na_v inactivation. Wild-type FHF1B ($n = 10$ cells) did not significantly shift $V_{1/2}$ inactivation compared to cells without FHF ($n = 10$), whereas $FHF1B_{R52H}$ ($n = 16$) induced a 15-mV depolarizing shift in $V_{1/2}$ ($p < .000005$). (B) Ectopic $FHF1B_{R52H}$ in cardiomyocytes slows rate of Na_v inactivation. For all cells described in A, sodium current decline at different membrane voltages was used to calculate the exponential τ (ms) for inactivation rate. At all test voltages, sodium channel inactivation rates in cells expressing $FHF1B_{R52H}$was reduced over two-fold compared to inactivation rates in cells expressing either wild-type FHF1B or no FHF ($p < .00005$). (C) Representative cardiac waveforms in a wild-type mouse. (D) Representative cardiac waveforms in a *Fhf1*$^{R52H/+}$ mouse prior to seizure. No significant difference was seen compared to wild-type (C). (E) Basal heart rates in wild-type and *Fhf1*$^{R52H/+}$ mice. No significant difference was seen. (F) PR intervals in wild-type and *Fhf1*$^{R52H/+}$ mice. No significant difference was seen. bpm, beats per minute; ECG, electrocardiogram

consequence of the *Fhf1*^{R52H} mutation, and not due to a hypothetical off-target mutation during CRISPR editing.

In humans, two siblings first described with EIEE and *FHF1*$^{R52H/+}$ genotype (EIEE47) died at 3 and 7 years of age,[22] potentially as a reflection of SUDEP, whereas nine other patients with the same de novo mutation also suffer from EIEE but have so far survived to between 3 and 32 years of age.[23–26] These clinical data stand in contrast to the fully penetrant EIEE and SUDEP phenotype of the *Fhf1*^{R52H} mutation in inbred mice. The heterogeneity of clinical course among individuals with the EIEE47 mutation may reflect a combination of variable genetic backgrounds and therapeutic treatment regimens employed at different institutions.

A fundamental question regarding SUDEP is whether seizure or postictal suppression compromises respiration, cardiac rhythm, or both.[1–8,11,20] In the *Fhf1*$^{R52H/+}$ mouse, heart rhythm is abruptly slowed within seconds of seizure onset. Bradycardia is likely triggered by a seizure-induced autonomic imbalance that causes or contributes to death, which in other mouse models is secondary to a wave of brain stem spreading depolarization following seizure onset.[8] As this study did not include measurement of respiration, it is possible that SUDEP in *Fhf1*$^{R52H/+}$ mice stems from a combination of cardiac and respiratory suppression during seizures. The tonic extension displayed during all observed *Fhf1*$^{R52H/+}$ seizures (Figure 3B, Video S2) may constitute a sustained mechanical impediment to breathing[47] coincident with bradycardia. Alternatively, analogous to other animal models,[48] the brain stem depolarization wave may also suppress activity in the pre-Botzinger complex breathing center, causing apnea that contributes to death.

The *Fhf1* gene is expressed in mouse atrium as well as the brain,[28,45] and we show here that ectopically expressed FHF1B$_{R52H}$ substitution is gain-of-function with respect to the modulation of cardiac sodium channel inactivation, paralleling prior findings regarding brain Na$_v$1.6 modulation.[22] However, heart rhythm in *Fhf1*$^{R52H/+}$ mice prior to seizure is apparently normal, at least for the readily measurable parameters of heart rate and PR interval. Atrial FHF1B$_{R52H}$ expression level in *Fhf1*$^{R52H/+}$ mice may not be sufficient to substantially alter Na$_v$ gating and conduction due to heterozygosity, endogenous coexpression of FHF2,[28] and a potentially less than 1:1 stoichiometry of FHF:Na$_v$. Furthermore, potentially small effects on the P wave in *Fhf1*$^{R52H/+}$ mice may have escaped our detection with single chest electrode ECG.

The *Fhf1*$^{R52H/+}$ and *Scn8a*$^{N1768D/+}$ mouse phenotypes are remarkably similar, reflecting the related effects of these mutations on Na$_v$1.6 gating and the broadly distributed expression of both genes in the brain, including principle excitatory cortical neurons. Both mutants undergo SUDEP at 2–4 weeks of age[16,19] (and this study) accompanied by apparent autonomic-mediated bradycardia[19] (and this study), and both mutations induce large depolarizing shifts in the voltage dependence of Na$_v$1.6 inactivation.[13,22] These similarities warrant consideration of *SCN8A* EIEE13 and *FHF1* EIEE47 as mechanistically related gain-of-function epilepsies.

ACKNOWLEDGMENTS

Mice used in this study were produced by the Mouse Genetics and Gene Targeting CoRE at the Icahn School of Medicine at Mount Sinai, which is supported by the Tisch Cancer Institute at Mount Sinai (P30 CA196521, Cancer Center Grant Support). In particular, the authors would like to acknowledge the contributions of Kasper Bonderup in the in vitro fertilization generation of offspring for analysis. This research was supported in part by National Institutes of Health (NIH) R01NS092786 to J.V., NIH F31HL132438 to A.S., NIH R01HL105983, NIH R01HL142498, and a grant from the LeDucq Foundation to G.I.F., and City University of New York awards 608100048, 802330016, and 945850101 to M.G.

CONFLICT OF INTEREST

L.V. received support from Anavex Life Sciences, Amzell Biopharma, and Aequus Biopharma for projects unrelated to this study. LV is on the scientific advisory board of Mallinckrodt Pharmaceuticals. None of the other authors has any conflict of interest to disclose.

AUTHOR CONTRIBUTIONS

Jana Velíšková, Christopher Marra, Yue Liu, Akshay Shekhar, David S. Park, Glenn I. Fishman, Libor Velíšek, and Mitchell Goldfarb designed experiments. All authors performed experiments and acquired data. Jana Velíšková, Christopher Marra, Libor Velíšek, and Mitchell Goldfarb analyzed data. Jana Velíšková, Libor Velíšek, and Mitchell Goldfarb wrote the paper.

ORCID

Jana Velíšková https://orcid.org/0000-0001-6094-7210
Christopher Marra https://orcid.org/0000-0003-4647-305X
Glenn I. Fishman https://orcid.org/0000-0002-2366-8527
Libor Velíšek https://orcid.org/0000-0003-2805-349X
Mitchell Goldfarb https://orcid.org/0000-0002-7219-7645

REFERENCES

1. Jehi L, Najm IM. Sudden unexpected death in epilepsy: impact, mechanisms, and prevention. Cleve Clin J Med. 2008;75(Suppl 2):S66–70.
2. Tolstykh GP, Cavazos JE. Potential mechanisms of sudden unexpected death in epilepsy. Epilepsy Behav. 2013;26:410–4.
3. Kalume F, Westenbroek RE, Cheah CS, Yu FH, Oakley JC, Scheuer T, et al. Sudden unexplained death in a mouse model of Dravet syndrome. J Clin Invest. 2013;123:1798–808.
4. Auerbach DS, Jones J, Clawson BC, Offord J, Lenk GM, Ogiwara I, et al. Altered cardiac electrophysiology and SUDEP in a model of Dravet syndrome. PLoS One. 2013;8:e77843.

5. Kim Y, Bravo E, Thirnbeck CK, Smith-Mellecker LA, Kim SH, Gehlbach BK, et al. Severe peri-ictal respiratory dysfunction is common in Dravet syndrome. J Clin Invest. 2018;128:1141–53.
6. Dlouhy BJ, Gehlbach BK, Richerson GB. Sudden unexplained death in epilepsy: basic mechanisms and clinical implications for prevention. J Neurol Neurosurg Psychiatry. 2016;87:402–13.
7. Shoemaker JK, Goswami R. Forebrain neurocircuitry associated with human reflex cardiovascular control. Front Physiol. 2015;6:240.
8. Aiba I, Noebels JL. Spreading depolarization in the brainstem mediates sudden cardiorespiratory arrest in mouse SUDEP models. Sci Transl Med. 2015;7(282):282ra46.
9. Escayg A, MacDonald BT, Meisler MH, Baulac S, Huberfeld G, An-Gourfinkel I, et al. Mutations of *SCNA1*, encoding a neuronal sodium channel, in two families with GEFS+2. Nat Genet. 2000;24:343–5.
10. Marini C, Scheffer IE, Nabbout R, Suls A, De Jonghe P, Zara F, et al. The genetics of Dravet syndrome. Epilepsia. 2011;52(Suppl 2):24–9.
11. Kuo F-S, Cleary CM, LoTurco JJ, Chen X, Mulkey DK. Disordered breathing in a mouse model of Dravet syndrome. eLife. 2019;8:e43387.
12. Rubinstein M, Han S, Tai C, Westenbroek RE, Hunker A, Scheuer T, et al. Dissecting the phenotypes of Dravet syndrome by gene deletion. Brain. 2015;138:2219–33.
13. Veeramah KR, O'Brien JE, Meisler MH, Cheng X, Dib-Hajj SD, Waxman SG, et al. De novo pathogenic *SCN8A* mutation identified by whole genome sequencing of a family quartet affected by infantile epileptic encephalopathy and SUDEP. Am J Hum Genet. 2012;90:502–10.
14. Ohba C, Kato M, Takahashi S, Lerman-Sagie T, Lev D, Terashima H, et al. Early onset epileptic encephalopathy caused by de novo *SCN8A* mutations. Epilepsia. 2014;55:994–1000.
15. Xiao Y, Jiong J, Mao M, Liu L, Xingfang JL, Luo H, et al. Early-onset epileptic encephalopathy with de novo *SCN8A* mutation. Epilepsy Res. 2018;139:9–13.
16. Lopez-Santiago LF, Yuan Y, Wagnon JL, Hull JM, Frasier CR, O'Malley HA, et al. Neuronal hyperexcitability in a mouse model of *SCN8A* epileptic encephalopathy. Proc Natl Acad Sci U S A. 2017;114:2383–8.
17. Wagnon JL, Barker BS, Hounshell JA, Haaxma CA, Shealy A, Moss T, et al. Pathogenic mechanism of recurrent mutations of *SCN8A* in epileptic encephalopathy. Ann Clin Transl Neurol. 2016;3:114–23.
18. Estacion M, O'Brien JE, Conravey A, Hammer MF, Waxman SG, Dib-Hajj SD, et al. A novel de novo mutation of *SCN8A* ($Na_v1.6$) with enhanced channel activation in a child with epileptic encephalopathy. Neurobiol Dis. 2014;69:117–24.
19. Wagnon JL, Korn MJ, Parent R, Tarpey TA, Jones JM, Hammer MF, et al. Convulsive seizures and SUDEP in a mouse model of *SCN8A* epileptic encephalopathy. Hum Mol Genet. 2014;24:506–15.
20. Frasier CR, Wagnon JL, Bao YO, McVeigh LG, Lopez-Santiago LF, Meisler MH, et al. Cardiac arrhythmia in a mouse model of sodium channel *SCN8A* epileptic encephalopathy. Proc Natl Acad Sci U S A. 2016;113:12838–43.
21. Patino GA, Claes LRF, Lopez-Santiago LF, Slat EA, Dondeti RSR, Chen C, et al. A functional null mutation of *SCN1B* in a patient with Dravet syndrome. J Neurosci. 2009;29:10764–78.
22. Siekierska A, Isrie M, Liu Y, Scheldeman C, Vanthillo N, Lagae L, et al. Gain-of-function *FHF1* mutation causes early-onset epileptic encephalopathy with cerebellar atrophy. Neurology. 2016;86:2162–70.
23. Al-Mehmadi S, Splitt M, Ramesh V, DeBrosse S, Dessoffy K, Xia F, et al. FHF1 (FGF12) epileptic encephalopathy. Neurol Genet. 2016;2:e115.
24. Guella I, Huh L, McKenzie MB, Toyota EB, Bebin EM, Thompson ML, et al. De novo *FGF12* mutation in 2 patients with neonatal-onset epilepsy. Neurol Genet. 2016;2:e120.
25. Villeneuve N, Abidi A, Cacciagli P, Mignon-Ravix C, Chabrol B, Villard L, et al. Heterogeneity of FHF1 related phenotype: novel case with early attacks of apnea, partial mitochondrial respiratory chain complex II deficiency, neonatal onset seizures without degeneration. Eur J Paediatr Neurol. 2017;21:783–6.
26. Zhang L, Gao J, Liu H, Tian Y, Zhang X, Lei W, et al. Pathogenic variants identified by whole exome sequencing in 43 patients with epilepsy. Hum Genomics. 2020;14:44.
27. Smallwood PM, Munoz-Sanjuan I, Tong P, Macke JP, Hendry SHC, Gilbert DJ, et al. Fibroblast growth factor (FGF) homologous factors: new members of the FGF family implicated in nervous system development. Proc Natl Acad Sci U S A. 1996;93:9850–7.
28. Hartung H, Feldman B, Lovec H, Coulier F, Birnbaum D, Goldfarb M. Murine FGF-12 and FGF-13: expression in embryonic nervous system, connective tissue, and heart. Mech Dev. 1997;64:31–9.
29. Wang Q, McEwen DG, Ornitz DM. Subcellular and developmental expression of alternatively spliced forms of fibroblast growth factor 14. Mech Dev. 2000;90:283–7.
30. Goldfarb M, Schoorlemmer J, Williams A, Diwakar S, Wang Q, Huang X, et al. Fibroblast growth factor homologous factors control neuronal excitability through modulation of voltage-gated sodium channels. Neuron. 2007;55:449–63.
31. Venkatesan K, Liu Y, Goldfarb M. Fast-onset long-term open-state block of sodium channels by A-type FHFs mediates classical spike accommodation in hippocampal pyramidal neurons. J Neurosci. 2014;34:16126–39.
32. Lein ES, Hawrylycz MJ, Ao N, Ayres M, Bensinger A, Bernard A, et al. Genome-wide atlas of gene expression in the adult mouse brain. Nature. 2007;445:168–76.
33. Uhlén M, Fagerberg L, Hallström BM, Lindskog C, Oksvold P, Mardinoglu A, et al. Tissue-based map of the human proteome. Science. 2015;347:1260419.
34. Munoz-Sanjuan I, Smallwood PM, Nathans J. Isoform diversity among fibroblast growth factor homologous factors is generated by alternative promoter usage and splicing. J Biol Chem. 2000;275:2589–97.
35. Olsen S, Garbi M, Zampieri N, Eliseenkova AV, Ornitz DM, Goldfarb M, et al. Fibroblast growth factor (FGF) homologous factors share structural but not functional homology with FGFs. J Biol Chem. 2003;278:34226–36.
36. Goetz R, Dover K, Laezza F, Shtraizent N, Huang X, Tchetchik D, et al. Crystal structure of a fibroblast growth factor homologous factor (FHF) defines a conserved surface on FHFs for binding and modulation of voltage-gated sodium channels. J Biol Chem. 2009;284:17883–96.
37. Wang C, Chung BC, Yan H, Lee S-Y, Pitt GS. Crystal structure of the ternary complex of a NaV C-terminal domain, a fibroblast growth factor homologous factor, and calmodulin. Structure. 2012;20:1167–76.
38. Yang H, Wang H, Shivalila CS, Cheng AW, Shi L, Jaenisch R. One-step generation of mice carrying reporter and conditional

alleles by CRISPR/Cas-mediated genome engineering. Cell. 2013;154:1370–9.
39. Ran FA, Hsu PD, Lin C-Y, Gootenberg JS, Konermann S, Trevino AE, et al. Double nicking by RNA-guided CRISPR Cas9 for enhanced genome editing specificity. Cell. 2013;154:1380–9.
40. Velíšek L, Shang E, Velíšková J, Chachua T, Macchiarulo S, Maglakelidze G, et al. GABAergic neuron deficit as an idiopathic generalized epilepsy mechanism: the role of BRD2 haploinsufficiency in juvenile myoclonic epilepsy. PLoS One. 2011;6:e23656.
41. Mishra V, Gautier NM, Glasscock E. Simultaneous video-EEG-ECG monitoring to identify neurocardiac dysfunction in mouse models of epilepsy. J Vis Exp. 2018;131:e57300.
42. He TC, Zhou S, da Costa LT, Yu J, Kinzler KW, Vogelstein B. A simplified system for generating recombinant adenoviruses. Proc Natl Acad Sci U S A. 1998;95:2509–14.
43. Park DS, Shekhar A, Marra C, Lin X, Vasquez C, Solinas S, et al. Fhf2 gene deletion causes temperature-sensitive cardiac conduction failure. Nat Commun. 2016;7:12966.
44. Wang C, Hennessey JA, Kirkton RD, Wang C, Graham V, Puranam RS, et al. Fibroblast growth factor homologous factor 13 regulates Na^+ channels and conduction velocity in murine hearts. Circ Res. 2011;109:775–82.
45. Wiencierz AM, Kernbach M, Ecklebe J, Monnerat G, Tomiuk S, Raulf A, et al. Differential expression levels of integrin α6 enable the selective identification and isolation of atrial and ventricular cardiomyocytes. PLoS One. 2015;10:e0143538.
46. Liu C, Dib-Hajj SD, Reganathan M, Cummins TR, Waxman SG. Modulation of the cardiac sodium channel $Na_v1.5$ by fibroblast growth factor homologous factor 1B. J Biol Chem. 2003;278:1029–36.
47. Nashef L, Walker F, Allen P, Sander JWAS, Shorvon SD, Fish DR. Apnoea and bradycardia during epileptic seizures: relationship to sudden death in epilepsy. J Neurol Neurosurg Psychiatry. 1996;60:297–300.
48. Jefferys JGR, Arafat AR, Irazoqui PP, Lovick TA. Brainstem activity, apnea, and death during seizures induced by intrahippocampal kainic acid in anaesthetized rats. Epilepsia. 2019;60:2346–58.

SUPPORTING INFORMATION

Additional supporting information may be found online in the Supporting Information section.

How to cite this article: Velíšková J, Marra C, Liu Y, et al. Early onset epilepsy and sudden unexpected death in epilepsy with cardiac arrhythmia in mice carrying the early infantile epileptic encephalopathy 47 gain-of-function *FHF1(FGF12)* missense mutation. *Epilepsia*. 2021;62:1546–1558. https://doi.org/10.1111/epi.16916